Journal of Alloys and Compounds 516 (2012) 96–101

Contents lists available at SciVerse ScienceDirect

Journal of Alloys and Compounds

journal homepage: www.elsevier.com/locate/jallcom

Quaternary Cu_2ZnSnS_4 nanocrystals: Facile and low cost synthesis by microwave-assisted solution method

Seung Wook Shin[a], Jun Hee Han[a], Chan Yeong Park[b], Annasaheb Vitthal Moholkar[c], Jeong Yong Lee[a,*], Jin Hyeok Kim[b,**]

[a] Department of Materials Science and Engineering, KAIST, 335 Gwahangno, Yuseong-gu, Daejeon 305-701, South Korea
[b] Photonics Technology Research Institute, Department of Materials Science and Engineering, Chonnam National University, 300 Yongbong-Dong, Buk-Gu, Gwangju 500-757, South Korea
[c] Department of Physics, Shivaji University, Kolhapur 416-004, India

ARTICLE INFO

Article history:
Received 27 October 2011
Accepted 28 November 2011
Available online 6 December 2011

Keywords:
Cu_2ZnSnS_4 (CZTS)
Nanocrystals
Photovoltaic
Facile and low cost process

ABSTRACT

Cu_2ZnSnS_4 (CZTS) nanocrystals (NCs), a promising alternative for In- and Ga-free absorber materials, were snythesized by a novel route using a two-step process. In the first step, the precursor powders were obtained by microwave irradiation at 700 W for 10 min from aqueous solutions containing copper, zinc, tin and sulfur elements. In the second step, the precursor powder was sulfurized by annealing in H_2S (5%) + N_2 (95%) atmosphere at 550 °C for 1 h. The structural, compositional, thermal and optical characteristics of CZTS NCs have been investigated. X-ray diffraction patterns, X-ray photoelectron spectroscopy and transmission electron microscopy results showed that the sulfurized NCs were a single kieserite CZTS phase without Cu_2SnS_3, ZnS, CuS and SnS secondary phases. Thermo-gravimetric analysis and differential-thermal analysis indicated a weight loss at about 840 °C and endothermic peak at same temperature from CZTS nature. Energy dispersive X-ray results showed that composition of CZTS NCs had a Cu and Zn-rich and S-poor. UV–vis spectroscopy results indicated that the absorption coefficient was over 10^4 cm^{-1} in the visible region. The direct band gap energy of the CZTS NCs estimated at about 1.5 eV, is ideal for its use in photovoltaic applications.

1. Introduction

Chalcogenide-based semiconductors, such as $CuInSe_2$ (CIS), $CuGaSe_2$ (CGS), $Cu(In,Ga)Se_2$ (CIGS) and CdTe, have attracted considerable interest as the efficient materials in thin film solar cells (TFSCs) [1,2]. Currently, CIGS and CdTe TFSCs have demonstrated the highest power conversion efficiency (PCE) over 11% in module production [3,4]. However, commercialized CIGS and CdTe TFSCs have some limitations due to the scarcity of In, Ga and Te and the environmental issues associated with Cd and Se [5–7]. Therefore, it is necessary to develop the alternative to the In- and Ga-free absorber materials uniting of naturally abundant and non-toxic elements in the earth's crust to improve the PCE of the TFSCs devices. The copper-zinc-tin-chalcogen-based kesterite, i.e. Cu_2ZnSnS_4 (CZTS), is a promising candidate owing to its direct band gap energy of 1.5 eV and high absorption coefficient >10^4 cm^{-1} in visible wavelength region [8]. In addition, it contains less toxic material S as compared to Se [8]. Based on photon balance, Shockley and Queisser et al. [9] reported the theoretical limit of 32.2% efficiency for CZTS-based TFSCs indicating that one has to tailor the crucial properties of CZTS absorber material for the fabrication of low cost, efficient and high PCE TFSCs devices.

The literature survey indicates that CIGS- and CZTS-based TFSCs devices have the highest PCE of 19.9% for CIGS and 6.77% for CZTS based TFSCs using high vacuum techniques co-evaporation and sputtering, respectively [1,10]. However, these high vacuum techniques have some drawbacks such as high cost, vacuum requirement, temperature reliance, complicated apparatus and most importantly the formation of unwanted phases during deposition processes [11–14]. Moreover, the industrial throughput of TFSC devices is very limited to meet the energy demand of mankind over the globe [2]. To overcome the drawback and improve the PEC of the present solar cells and investigate other novel alternatives, many researchers have adopted non-vacuum approach owing to low cost and simple process which includes spin coating [11,15], drop coasting [13,14], doctor blade deposition [16], spray pyrolysis [17], sol–gel [18] and electro- and photochemical deposition [12,19–21]. Recently, Todorov et al. [22] have reported the highest PCE of 9.66% for CZTS-based TFSCs using the hybrid solution-particle approach. Although the CZTS TFSCs using

* Corresponding author. Tel.: +82 42 350 4216; fax: +82 42 350 3310.
** Corresponding author. Tel.: +82 62 530 1709; fax: +82 62 530 1699.
E-mail addresses: jinhyeok@chonnam.ac.kr (J.Y. Lee), j.y.lee@kaist.ac.kr (J.H. Kim).

0925-8388/$ – see front matter © 2011 Elsevier B.V. All rights reserved.
doi:10.1016/j.jallcom.2011.11.143

non-vacuum approach have several merits and high PCE, they suffer from various problems such as incorporation of undesired impurities (carbon, oxygen, binder reminder and solvent) and chemical toxicity (e.g. hydrazine hydrate) for scaling up massive solar cell production needs to be addressed [12]. In particular, the impurities in absorber layer and toxic chemicals are responsible for the low PCE and limited commercialization [2].

On the other hand, nanocrystals (NCs)-based absorber layer, are synthesized using solution-based techniques such as solvothermal [23], low temperature colloid method [16] and hot injection [24,25], have fascinated precise attention due to their low manufacturing costs, possibility of large scale and high throughput using roll to roll TFSCs fabrication processes. Recently, Guo et al. [26] reported on the fabrication of $Cu_2ZnSn(S,Se)_4$ (CZTSSe) TFSCs with a PCE of 7.2% using NCs in organic solvent under light soaking condition. Riha et al. [27], Shavel et al. [25] and Guo et al. [24] reported the synthesis of CZTS or CZTSSe NCs by hot injection solution method over 225 °C. The oleylamine or hexadecylamine has been used to stabilize the NCs in organic solvents. In addition, Steinhagen et al. [23] reported the synthesis of CZTS NCs by a solvothermal method at a temperature 280 °C using oleylamine and hexadecylamine as stabilizers. The PCE of the TFSCs fabricated using their CZTS NCs is about 0.23%. Although the shape and size of these CZTS NCs were uniform, the hazardous chemicals, such as oleylamine and hexadecylamine, have been required in the synthesis process. This issue has stimulated research community to investigate the hazard-chemical free solution-based process of CZTS NCs with adequate photovoltaic properties. This paper reports the synthesis of microwave-assisted CZTS NCs without hazard chemicals and post annealing effect on their properties.

The CZTS NCs were prepared using a two-step process. In the first step, the precursor powder was obtained from aqueous solution containing 40 mL of 0.2 M Cu acetate, 40 mL of 0.1 M Zn acetate, 40 mL of 0.1 M Sn chloride and 40 mL of 0.2 M thioacetamide at pH 7 that had been irradiated with microwave energy of 700 W for 10 min at room temperature. In the second step, the precursor powder was sulfurized in a tubular furnace system in N_2 (95%) + H_2S (5%) atmosphere at 550 °C for 1 h.

2. Experimental

2.1. Chemicals

Copper(II) acetate (Cu(OAc), 99.99%), zinc acetate (Zn(OAc), 99.99%), tin(IV) chloride ($SnCl_2$, 99.99%) and thioacetamide (TAA, 99.99%) were purchased from Aldrich and used as received.

2.2. Synthesis of precursor powders

The precursor solution was prepared using 40 mL of 0.2 M Cu(OAc), 40 mL of 0.1 M Zn(OAc) and 40 mL of 0.1 M $SnCl_2$. Subsequently, 40 mL of a 0.2 M TAA solution was added and the pH was adjusted to 7 by adding an ammonia (NH_4OH) solution with constant magnetic stirring for 10 min at room temperature. During this step, the color of the precursor solution changed from a transparent to a brown-green. The precursor solution was irradiated with microwave energy using a commercial microwave oven (KR-B200B, Daewoo, Korea) at 700 W for 10 min. After 6 min, the precursor solution was boiled and the color changed from brown-green to dark-blue. The reacted solution was then cooled to room temperature in air. The powder formed in the solution was separated from the precursor solution by centrifugation at 3000 rpm for 10 min. This process was repeated three times. Finally, the precursor powder was dried in a vacuum oven at 60 °C for 8 h.

2.3. Annealing process of powders

The precursor powder was annealed in a mixture gas of N_2 (95%) + H_2S (5%) at 550 °C for 1 h using a commercial furnace system. The heating and cooling rates were 10 °C/min. and 5 °C/min, respectively.

2.4. Characterizations

The crystallographic information of the nanocrystals (NCs) was obtained from the powder X-ray diffraction patterns (PXRD, PANalytical, X'Pert-PRO and Netherlands) operated at 45 kV and 40 mA. The bright-field (BF) transmission electron microscopy (TEM) images, their corresponding selected area electron diffraction (SAED) patterns, and high-resolution (HR) TEM images of the NCs were obtained using JEOL-3010 at an operating voltage of 300 kV. Elemental mapping images and energy-dispersive X-ray spectra were acquired by energy-dispersive X-ray spectroscopy (EDS) using a Tecnai G2 F30 installed in a scanning transmission electron microscopy (STEM) equipped with a high-angle annular dark-field (HAADF) unit. The simulated images of an atomic arrangement were also obtained using the National Center for Electron Microscopy Simulation Software (NCEMSS) from the Lawrence Berkeley National Laboratory. The compositional ratios of the NCs were analyzed by EDS attached to a field emission-scanning electron microscopy (FE-SEM, JMS-7500F, JEOL and Japan). The chemical binding energy of the annealed NCs was examined by high-resolution X-ray photoelectron spectroscopy (HR-XPS, VG Multilab 2000, Thermo VG Scientific and UK) at room temperature. The binding energies in the spectrometer were calibrated using the carbon 1 s line at 285.0 eV. Thermogravimetric/differential thermal analyses (TGA/DTA) of NCs were performed using a Ta Instruments 1600 DTA (USA) with a flowing nitrogen atmosphere from room temperature to 1100 °C. The optical absorption and band gap energy of the NCs were

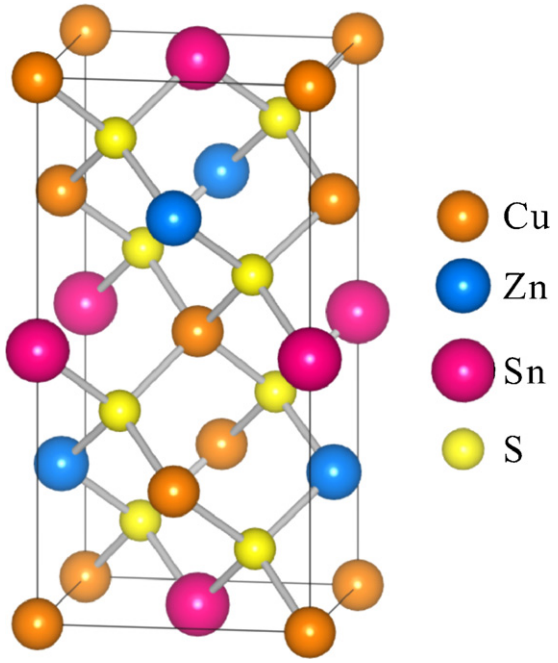

Fig. 1. A schematic diagram of kesterite CZTS illustrated by the Visualization for Electronic and Structural Analysis software.

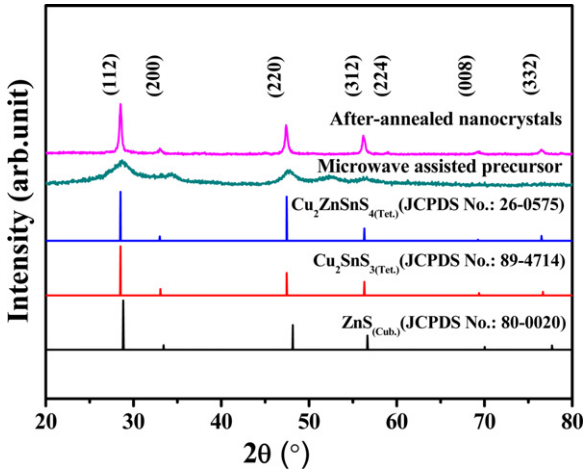

Fig. 2. PXRD patterns of the microwave assisted precursor and after-annealed CZTS NCs [Cu Kα radiation (λ = 1.54 Å)]. The peaks are indexed to the different planes according to tetragonal CZTS (JCPDS No.: 26-0575), tetragonal Cu_2SnS_3 (JCPDS No.: 89-4714), and cubic ZnS (JCPDS No.: 80-0020) structures, indicating that the three compounds have similar diffraction patterns.

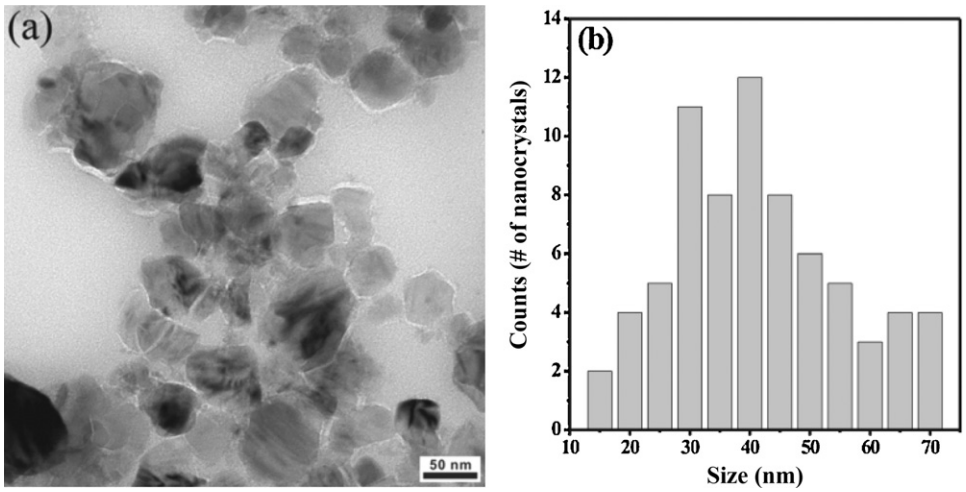

Fig. 3. Bright-field TEM image of the pre-annealed microwave assisted CZTS precursor powder and the corresponding size distribution plots. The CZTS NCs show a wide size distribution varying from 10 nm to 70 nm with an average size of 42.1 ± 12.7 nm.

measured by UV–visible spectroscopy (Cary 100, Varian, Mulgrave and Australia) at room temperature.

3. Result and discussions

Fig. 1 shows a schematic diagram of kesterite CZTS illustrated by the Visualization for Electronic and Structural Analysis software. The structure of CZTS is tetragonal kesterite in which each cation is bonded to four sulfurs anions and the cation layer alternate with the sulfur anion layer along the crystallographic c-direction as CuZn/SS/CuSn/SS are observed [24]. This structure is similar to the chalcopyrite structure of $CuInS_2$ in which cation and anion layers are alternate such as CuIn/SS/CuIn/SS [24].

Fig. 2 shows the powder X-ray diffraction (PXRD) patterns of the microwave-assisted precursor powder and post-annealed powder samples. The PXRD patterns of the microwave-assisted precursor showed several broad peaks that could not be assigned to CZTS, ZnS, $Cu_{2-x}S$, SnS and Cu_2SnS_3 (CTS) phases. On the other hand, the PXRD patterns of post-annealed powder show peaks corresponding to the (1 1 2), (2 0 0), (2 2 0), (3 1 2), (2 2 4), (0 0 8) and (3 3 2) planes

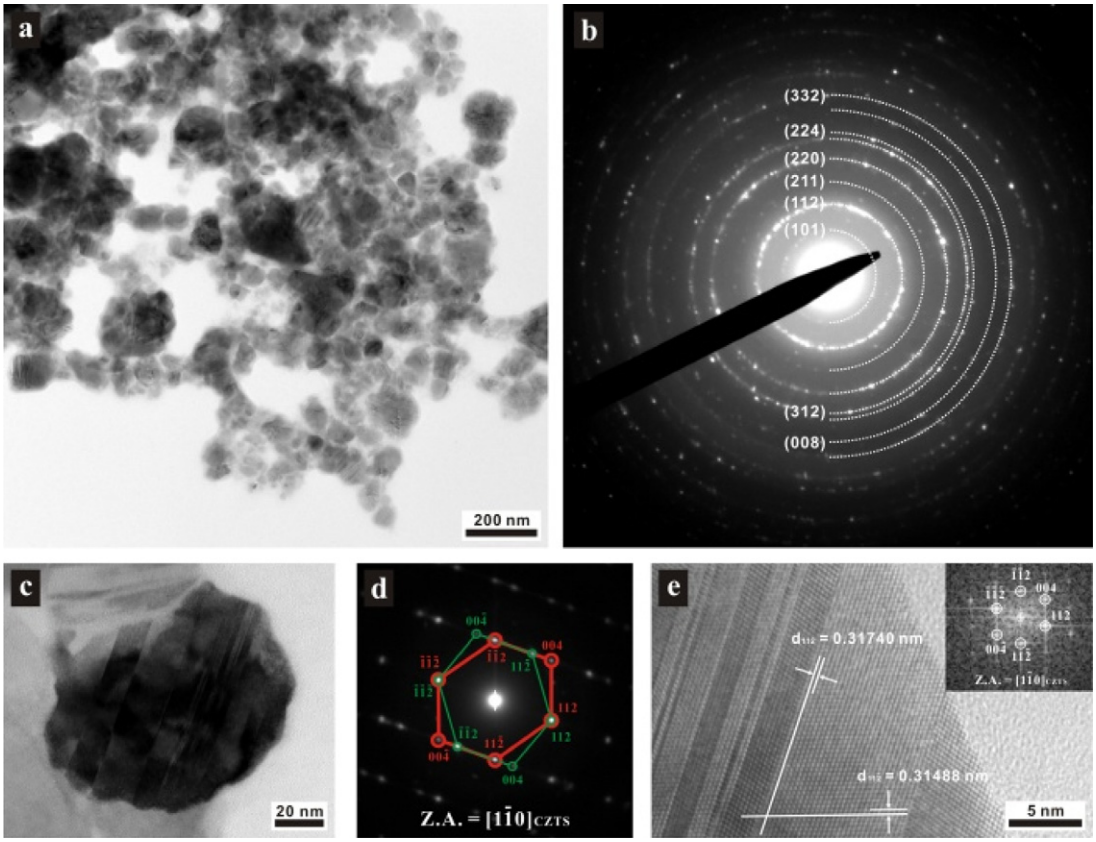

Fig. 4. BF-TEM images of post-annealed microwave assisted CZTS NCs (a), and its corresponding diffraction pattern (b). High-resolution TEM image of a twinned CZTS NC (c) and its corresponding SAED pattern with indexing (d). Magnified high-resolution TEM image (e) of CZTS NC of (c). The inset in (e) shows an indexed phase-Fourier transform image.

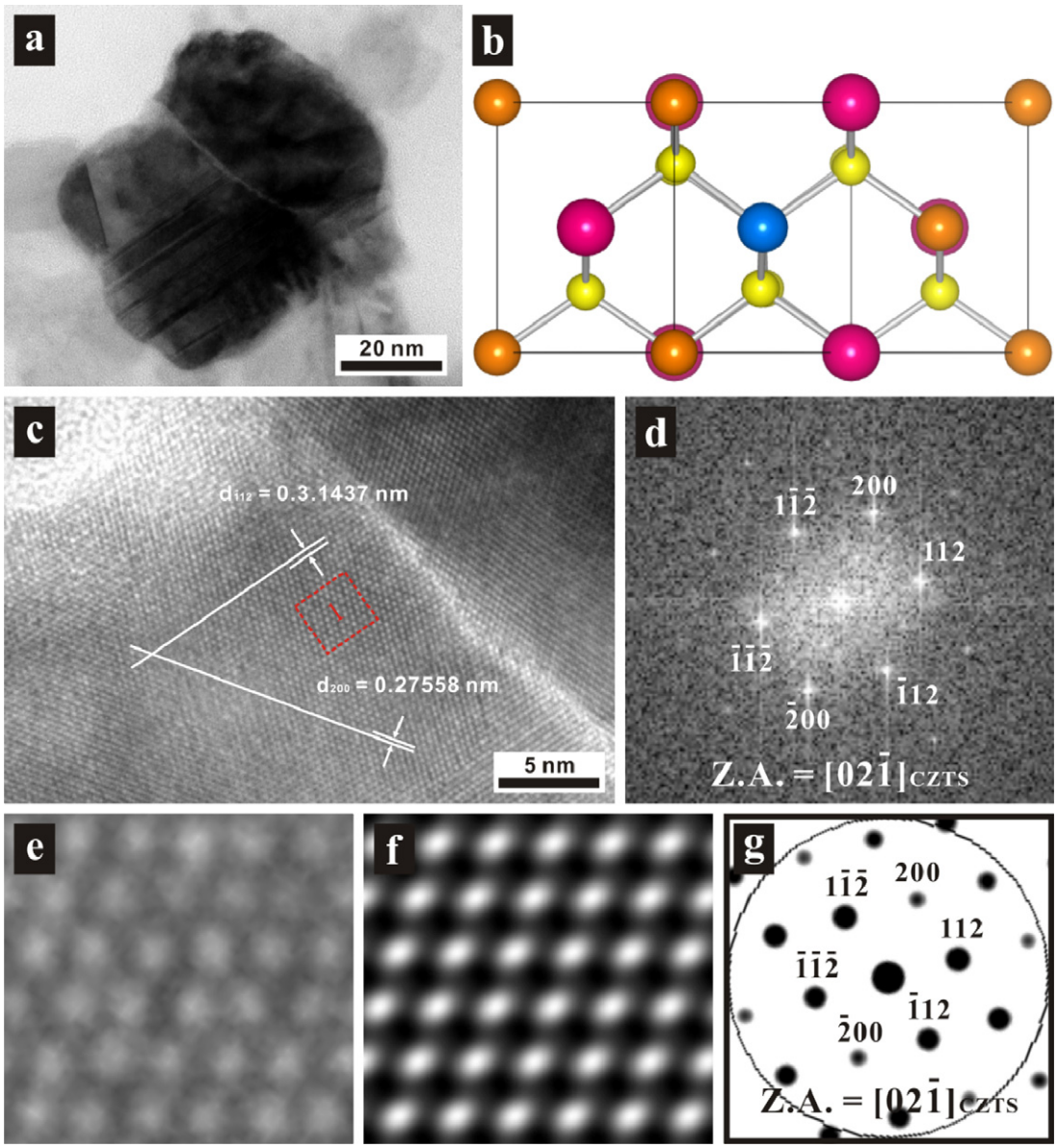

Fig. 5. BF-TEM image of CZTS NCs (a). A schematic diagram of the crystal structure of kesterite CZTS projected along $[02\bar{1}]$ direction (b). HR-TEM image of CZTS NCs (c) in (a), and fast-Fourier transform image (d) of the dashed square region in (c). The magnified image (e) of the dashed square region in (c), its simulated lattice image (f) under the conditions of 30 Å thickness and 50 Å defocus and diffraction pattern (g).

of a single kesterite-type CZTS structure (JCPDS No.: 26-0575). A shoulder observed to the left of the (1 1 2) plane might have originated from a stacking faults related to cation disordering similar to the faults observed in $CuInSe_2$ and CIGS [24]. The values of lattice parameters are $a = 5.42$ Å and $c = 10.84$ Å and are in good agreement with the kesterite-type CZTS structure [8].

Fig. 3 shows a bright-field (BF)-TEM image of pre-annealed microwave assisted CZTS powder (a) and the corresponding size distribution plots (b). The BF-TEM image showed that CZTS NCs are of irregular and faceted shapes. The diameter of the CZTS NCs varies from 10 nm to 70 nm and average diameter of CZTS NCs is 42.1 ± 12.7 nm. The CZTS NCs have wide grain size distribution of 30%.

Fig. 4 shows the BF-TEM image of the post-annealed microwave assisted CZTS powder (a) along with its corresponding diffraction pattern (b). The ring patterns obtained from the polycrystalline materials shown in Fig. 4(b) can be indexed to the (1 0 1), (1 1 2), (2 1 1), (2 2 0), (2 2 4) and (3 3 2) planes of a kesterite-type CZTS phase, which is consistent with the PXRD pattern shown in Fig. 2. Since the PXRD pattern and ring pattern from TEM does not clearly suggest the formation of either CTS or ZnS with a CZTS phase, therefore, an additional diffraction pattern and high-resolution (HR)-TEM analysis of one NC focused on the crystallographic points has been carried out (Fig. 4(c)). The magnified BF-TEM image shows one NC and its corresponding selected area electron diffraction (SAED) pattern (Fig. 4(d)) obtained from Fig. 4(a). The SAED pattern is well indexed to the kesterite-type CZTS projected along the $[1\,\bar{1}\,0]$ direction. The HR-TEM image of the NC also shows the atomic arrangement of the CZTS phase with a d-spacing of 0.31740 nm and 0.31488 nm. The phase/fast Fourier transform image in the inset is also well consistent with the peaks indexed to the zone axis of the $[1\,\bar{1}\,0]$ direction, as shown in Fig. 4(e).

Fig. 5 shows the additional HR-TEM images of (a) schematic diagram of the crystal structure of kesterite CZTS projected along $[0\,2\,\bar{1}]$ direction (b), HR-atomic lattice image of one CZTS NC (c), fast-Fourier transform image (d), magnified image (e) of the dashed

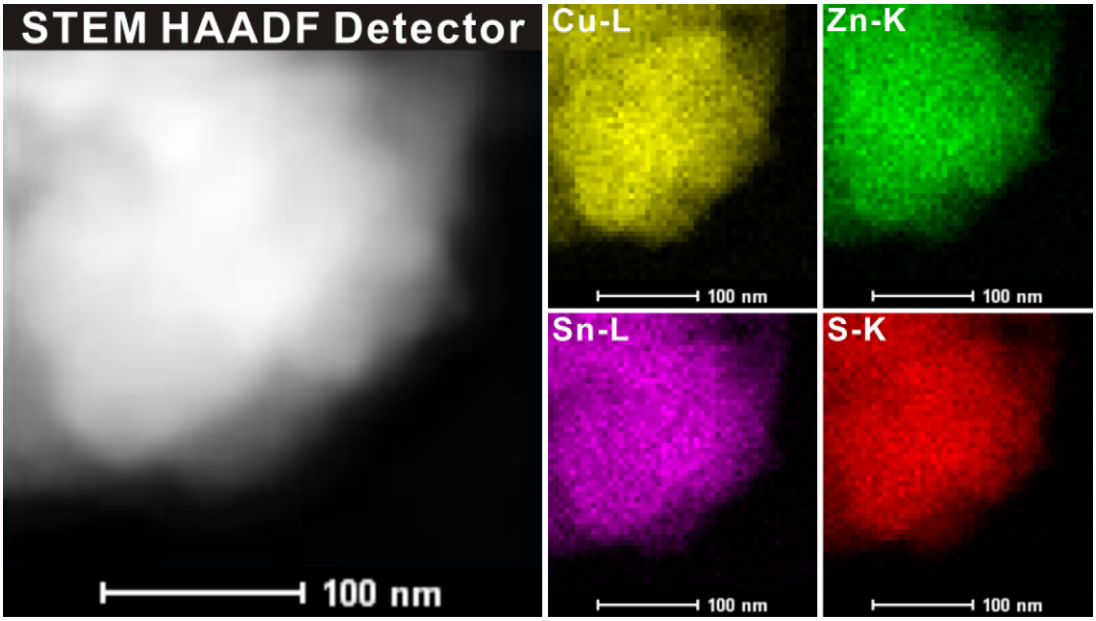

Fig. 6. HAADF-STEM image and elemental mapping images of CZTS NCs. The images were obtained on carbon film-assisted Ni grids (200 mesh, Electron Microscopy Sciences) using a Tecnia G2 F30 equipped with a high-angle annular dark-field (HAADF) unit at an accelerating voltage of 300 kV.

square region in (c), simulated lattice image (f) and diffraction patterns (g) of the CZTS NCs. It is also observed that there are many stacking faults in one CZTS NC (a) and these defects of CZTS NCs release is well supported by literature survey [23–26]. The observed values of atomic d-spacing (Fig. 5(c)) and diffraction patterns (Fig. 5(d)) are in good agreement with that of Fig. 4(e). The HR-atomic lattice image (c) and fast-Fourier transform image (d) from CZTS NC also matches with simulated lattice image (f) and diffraction patterns (g) obtained from the National Center for Electron Microscopy Simulation Software. These TEM and simulation results confirm that the NCs have a kesterite phase without any other secondary phases.

Fig. 6 shows the scanning transmission electron microscopy (STEM), energy-dispersive X-ray spectroscopy (EDS) elemental mapping equipped with a high angle annular dark field (HAADF) of CZTS NCs (Fig. 4). This analysis shows that Cu, Zn, Sn and S are well distributed in the NCs without any apparent element separation or aggregation. In addition, the EDS spectrum of the CZTS NCs

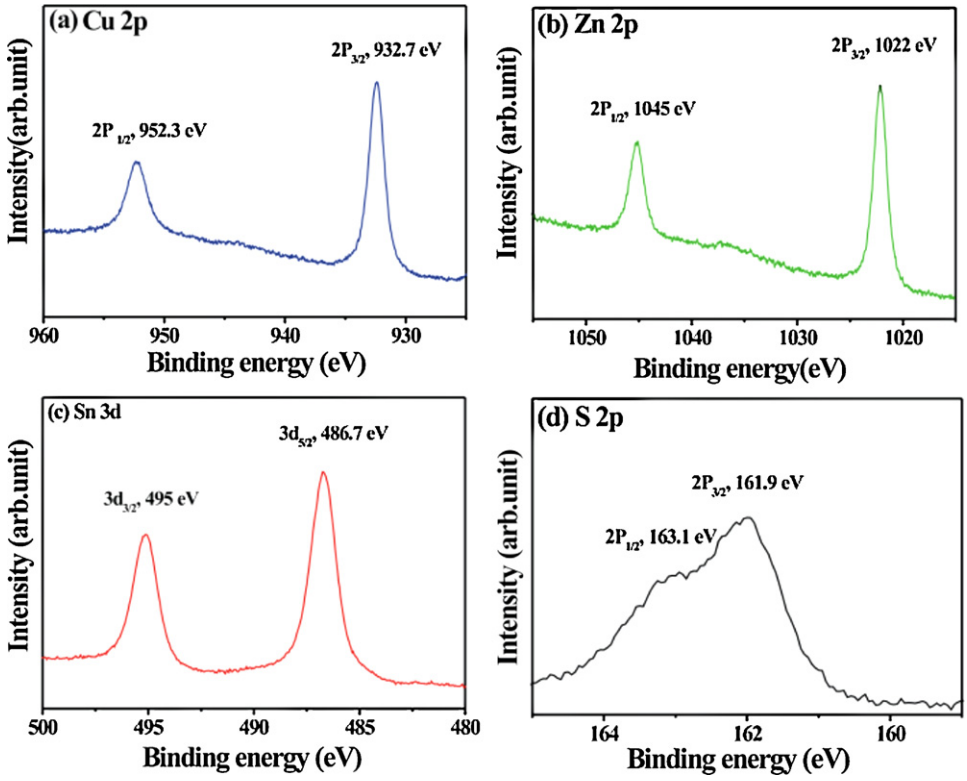

Fig. 7. High-resolution XP spectra of CZTS NCs; (a) Cu 2p, (b) Zn 2p, (c) Sn 3d, and S 2p core levels, respectively.

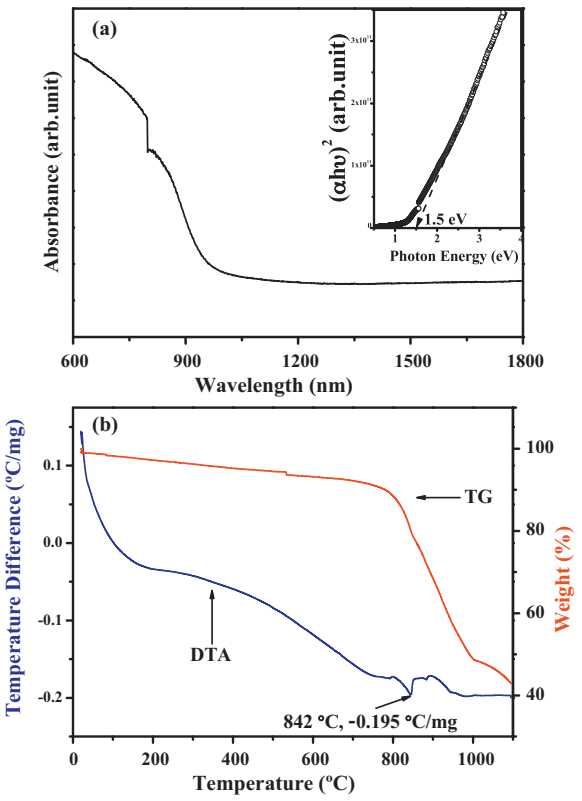

Fig. 8. UV–vis absorption spectrum (a) and TGA/DTA analysis (b) of CZTS NCs.

(shown not here) showed four elements including Cu, Zn, Sn and S. The relative elemental ratio of Cu:Zn:Sn:S is 2.8:1.7:1.1:4.2. The other occurred C and O peaks may be attributed to carbon adhesive tape.

HR XPS analysis has been performed to identify the phases of the NCs and the presence of four elements without secondary phases. Fig. 7 shows HR X-ray photoelectron spectroscopy (HR-XPS) analysis of the CZTS NCs. The Cu binding energy peaks of NCs observed at 932.7 eV and 952.3 eV corresponds to the electronic states of Cu $2p_{3/2}$ and $2p_{1/2}$ core level of the CZTS compound [20]. The Zn binding energy peak of NCs located at 1022.3 eV corresponds to the electronic states of Zn $2p_{3/2}$ of the CZTS compound [28]. The Sn $3d_{5/2}$ and $3d_{3/2}$ peaks of the CZTS NCs are located at 486.7 eV and 495 eV, respectively [29]. The observed binding energy peaks located at 161.9 eV and 163.1 eV matches well with the electronic state of S $2p_{3/2}$ and S $2p_{1/2}$ core levels of the CZTS compound [27].

Fig. 8 shows the UV–vis absorption spectrum (a), (with an inset image of band gap energy) and thermo-gravimetric analysis (TGA)/differential-thermal analysis (DTA) (b) of the CZTS NCs. The optical absorption coefficient of the CZTS NCs is $>10^4$ cm^{-1} in the visible region. The optical band gap energy of the CZTS NCs is estimated to be approximately 1.5 eV from a linear extrapolation on the *x*-axis of $(ahv)^2$ vs photon energy (Fig. 6(a)). This estimated band gap energy is consistent with the literature values of 1.45–1.6 eV, indicating a stable band gap energy value required for applications in TFSCs [5]. TGA and DTA (Fig. 8(b)) of CZTS NCs indicate a weight loss around 840 °C and an endothermic peak at the same temperature from the CZTS characteristic [27]. It is worth to mention that from the XRD, TEM, XPS, UV–vis and TGA/DTA studies that the CZTS NCs with a kesterite-type CZTS structure without CTS, ZnS, SnS_2 and CuS secondary phases can be synthesized using any hazard chemicals or complexing agent.

4. Conclusion

In conclusion, quaternary CZTS NCs can be synthesized by a facile and simple route involving the annealing of microwave-assisted precursors without using hazardous chemicals. XRD, TEM, XPS, and TGA/DTA results confirmed the kesterite type structure of the CZTS NCs with a wide size distribution of 30%. The STEM-EDS elemental mapping image reveals the presence of four elements in each individual NC. Although the high quality the CZTS NCs have been synthesized successfully, a through investigation with high PCE for the efficient TFSCs, i.e. the impact of deviated composition ratio and understanding the mechanism of irregular shape is necessarily required. Studies on optimizing the synthesis processes and other parameters through precise control of the composition ratio of the CZTS NCs along with the fabrication of CZTS-based TFSCs are currently underway.

Acknowledgment

This study was financially supported by National Research Foundation of Korea (NRF) grant funded by the Korean government (MEST-No. 2011-0016564).

References

[1] I. Contreras Repins, M.A. Egaas, B. DeHart, C. Scharf, J. Perkins, C.L. To, B. Noufi, Prog. Photovolt.: Res. Appl. 16 (2008) 235–239.
[2] D.B. Mitzi, Adv. Mater. 21 (2009) 3141–3158.
[3] A.A. Harry, P. Albert, Nat. Mater. 9 (2010) 205–213.
[4] M.A. Green, K. Emery, Y. Hishikawa, W. Warta, Prog. Photovolt.: Res. Appl. 19 (2011) 84–92.
[5] D.B. Mitzi, M. Yuan, W. Liu, A. Kellock, J. Chey, S.J.V. Deline, A.G. Schrott, Adv. Mater. 20 (2008) 3657–3662.
[6] H. Katagiri, Thin Solid Films 480 (2005) 426–432.
[7] H. Katagiri, K. Jimbo, W. Maw, S.K. Oishi, M. Yamazaki, H. Araki, A. Takeuchi, Thin Solid Films 517 (2009) 2455–2460.
[8] D.B. Mitzi, T.K. Todorov, K. Wang, S. Guha, Sol. Energy Mater. Sol. Cells 95 (2011) 1421–1436.
[9] W. Shockley, H.J. Queisser, J. Appl. Phys. 32 (1961) 510–519.
[10] H. Katagiri, K. Jimbo, S. Yamada, T. Kamimura, W.S. Maw, T. Fukano, T. Fukano, T. Ito, T. Motohiro, Appl. Phys. Exp. 1 (2008) 041201–041202.
[11] W. Liu, D.B. Mitzi, M. Yuan, A.J. Kellock, S.J. Chey, O. Gunawan, Chem. Mater. 22 (2009) 1010–1014.
[12] C.J. Hibberd, E. Chassaing, W. Liu, D.B. Mitzi, D. Lincot, A.N. Tiwari, Prog. Photovolt.: Res. Appl. 18 (2010) 434–452.
[13] Q. Guo, G.M. Ford, H.W. Hillhouse, R. Agrawal, Nano Lett. 9 (2009) 3060–3065.
[14] Q. Guo, S.J. Kim, M. Kar, W.N. Shafarman, R.W. Birkmire, E.A. Stach, R. Agrawal, H.W. Hillhouse, Nano Lett. 8 (2008) 2982–2987.
[15] T.K. Todorov, E. Cordoncillo, J.F. Sánchez-Royo, J. Carda, P. Escribano, Chem. Mater. 18 (2006) 3145–3150.
[16] S.J. Ahn, C. Kim, J.H. Yun, J.H. Gwak, S. Jeong, B.H. Ryu, K.H. Yoon, J. Phys. Chem. C 114 (2010) 8108–8113.
[17] Y.B.K. Kumar, G.S. Babu, P.U. Bhaskar, V.S. Raja, Phys. Status Solidi A 206 (2009) 1525–1530.
[18] Y. Miyamoto, K. Tanaka, M. Oonuki, N. Moritake, H. Uchiki, Jpn. J. Appl. Phys. 47 (2008) 596–601.
[19] S.M. Pawar, B.S. Pawar, A.V. Moholkar, D.S. Choi, J.H. Yun, J.H. Moon, S.S. Kolekar, J.H. Kim, Electrochim. Acta 55 (2010) 4057–4061.
[20] B.S. Pawar, S.M. Pawar, S.W. Shin, D.S. Choi, C.J. Park, S.S. Kolekar, J.H. Kim, Appl. Surf. Sci. 257 (2010) 1786–2569.
[21] A. Ennaoui, M. Lux-Steiner, A. Weber, D. Abou-Ras, I. Kotschau, H.W. Schock, R. Schurr, A. Holzing, S. Jost, R. Hock, T. Voss, J. Schulze, A. Kirbs, Thin Solid Films 517 (2009) 2511–2514.
[22] T.K. Todorov, K.B. Reuter, D.B. Mitzi, Adv. Mater. 22 (2010) E156–E159.
[23] C. Steinhagen, M.G. Panthani, V. Akhavan, B. Goodfellow, B. Koo, B.A. Korgel, J. Am. Chem. Soc. 131 (2009) 12554–12555.
[24] Q. Guo, H.W. Hillhouse, R. Agrawal, J. Am. Chem. Soc. 131 (2009) 11672–11673.
[25] A. Shavel, J. Arbiol, A. Cabot, J. Am. Chem. Soc. 132 (2010) 4514–4515.
[26] Q. Guo, G.M. Ford, W.C. Yang, B.C. Walker, E.A. Stach, H.W. Hillhouse, R. Agrawal, J. Am. Chem. Soc. 132 (2010) 17384–17386.
[27] S.C. Riha, B.A. Parkinson, A.L. Prieto, J. Am. Chem. Soc. 131 (2009) 12054–12055.
[28] M. Cao, Y. Shen, J. Cryst. Growth 318 (2011) 1117–1120.
[29] V.G. Rajeshmon, C.S. Kartha, K.P. Vijayakumar, C. Sanjeeviraja, T. Abe, Y. Kashiwaba, Sol. Energy 85 (2011) 249–255.